ELSEVIER

Polymer 44 (2003) 143–155

polymer

www.elsevier.com/locate/polymer

# Thermally stable crosslinked NLO materials based on maleimides

Ru-Jong Jeng[a,*], Chia-Cheng Chang[a], Chih-Ping Chen[a], Chin-Ti Chen[b], Wen-Chiung Su[c]

[a]*Department of Chemical Engineering, National Chung Hsing University, Taichung 402, Taiwan, ROC*
[b]*Institute of Chemistry, Academia Sinica, Taipei 115, Taiwan, ROC*
[c]*Chung-Shan Institute of Science and Technology, Lungtan, Tauyuan 325, Taiwan, ROC*

Received 28 June 2002; received in revised form 6 September 2002; accepted 7 October 2002

**Abstract**

A series of thermally stable second-order nonlinear optical (NLO) polymeric materials based on bismaleimide chemistry have been developed. Two maleimide containing chromophores with excellent thermal stability were incorporated into the bismaleimide polymer matrices to form interpolymer networks. Moreover, a full interpenetrating polymer network (IPN) was formed through simultaneous addition reaction of the bismaleimide, and sol–gel process of alkoxysilane dyes (ASD). Atomic force microscopy results indicate that the inorganic networks are distributed throughout the polymer matrices on the molecular scale. The silica particle sizes are well under 200 nm. Second harmonic coefficients, $d_{33}$ of 6.9–57.0 pm/V have been obtained for the organic and organic/inorganic materials. Excellent temporal stability was obtained for these NLO materials at 100 °C. The dynamic thermal and temporal stabilities of the IPN system were much better than those of the crosslinked organic systems.


*Keywords:* Nonlinear optics; Bismaleimide; Sol–gel process

## 1. Introduction

There has been great interest in the development of second-order nonlinear optical (NLO) polymeric materials for photonics applications [1,2]. A number of NLO polymers have been developed to exhibit large second harmonic coefficients, comparable to those of the inorganic NLO materials which are currently in use in devices. However, the major drawback of NLO polymers that prevents them from being employed in device applications is the decay of electric field induced second-order optical nonlinearity. This decay is caused by the relaxation of the NLO chromophores from the induced acentric alignment to a random fashion. To prevent the randomization of the poled order, NLO chromophores are usually incorporated into high glass transition temperature ($T_g$) polymers and/or crosslinked polymer networks [3–9].

Aromatic polyimides are well-known for their high temperature stability and high glass transition temperatures [10]. Several approaches have been reported to enhance the stability and processability of NLO materials based on polyimides [11–14]. Jeng and coworkers have reported a second-order NLO organic/inorganic composite based on an alkoxysilane dye (ASD) and an aromatic polyimide [12]. Polyimide films containing a homogeneous dispersion of nano-sized $SiO_2$ particles have been achieved by means of a sol–gel process. The incorporation of an inorganic sol–gel material provides an inert environment for the polyimide and theoretically will prevent its thermal decomposition. The inorganic networks will be densely and uniformly packed throughout the organic chain segments by the sol–gel process [15–17]. Apart from high $T_g$'s of polyimides, the interactions between inorganic oxide particles and polyimide will reduce the molecular motions during the glass transition [17]. Therefore, the incorporation of an inorganic NLO sol–gel material within an organic polymer can effectively enhance long-term NLO stability at elevated temperatures.

On the basis of the above considerations, polyimides possessing both high $T_g$'s and crosslinked networks indeed seem to be a rational approach to enhance the NLO stability. Addition-type polyimides may be used to circumvent the need for thermal imidization. Improved processability is achieved without sacrificing useful properties, such as excellent thermal stability and mechanical properties [13,18–21]. Moreover, one can develop maleimide- or

* Corresponding author. Tel.: +886-4-2285-2581; fax: +886-4-2285-4734.
*E-mail address:* rjjeng@dragon.nchu.edu.tw (R.-J. Jeng).

0032-3861/03/$ - see front matter © 2002 Elsevier Science Ltd. All rights reserved.
PII: S0032-3861(02)00730-9

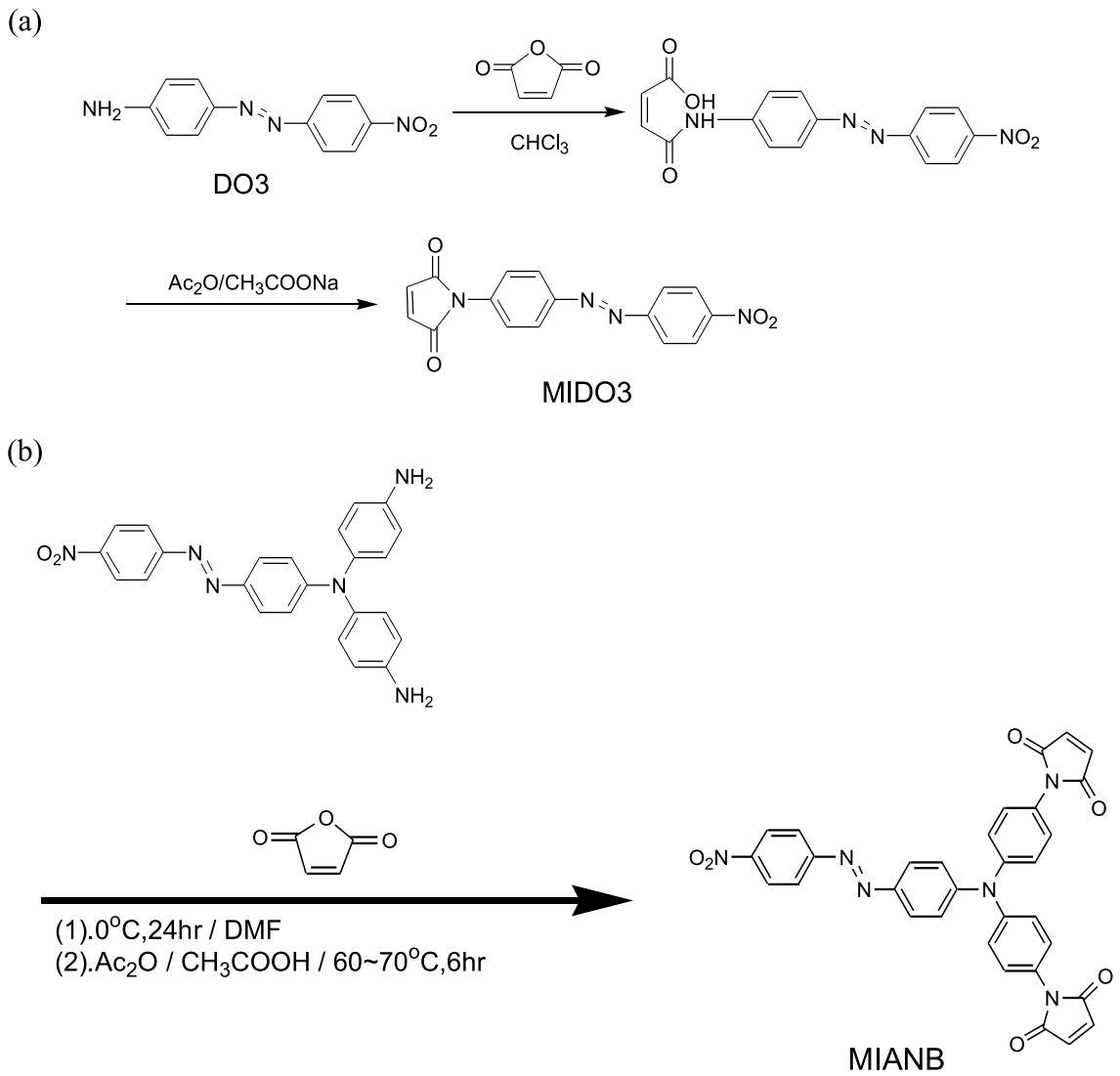


Scheme 1. Synthesis of the maleimide containing chromophores (a) MIDO3 and (b) MIANB.

alkoxysilane-attaching NLO chromophores to lead to highly crosslinked NLO-active polybismaleimides, or polybismaleimide/inorganic interpenetrating polymer networks (IPN), respectively. Especially the IPN is known to be able to remarkably suppress the creep and flow phenomena in polymers, and to promote compatibility between two polymers via simultaneous polymerization reactions [22]. The molecular motion of each polymer in IPN is restricted due to the entanglements between two different networks. These materials, with the hybrid properties of high $T_g$'s, extensively crosslinked networks, and permanent entanglements, would exhibit excellent temporal stability at elevated temperatures.

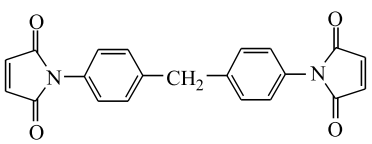

Fig. 1. Chemical structure of 4,4-(bismaleimido-diphenylmethane); BMI.

In this paper, we report an investigation of a crosslinked NLO-active polybismaleimide system, and an NLO-active IPN system consisting of a thermoset polybismaleimide and an NLO-active inorganic network. The crosslinked polybismaleimide system is based on maleimide containing chromophores (MIDO3 and MIANB; Scheme 1) and 4, 4′-(bismaleimido-diphenylmethane) (BMI; Fig. 1) via addition reaction. It is important to note that MIANB is a di-link NLO chromophore containing no flexible tether. The MIANB can be directly incorporated into the polybismaleimide matrices. The result is a rigid, functionalized donor-embedded crosslinked polybismaleimide with a high $T_g$ and exceptional thermal stability. On the other hand, the IPN system is based on a di-link bulky ASD (Scheme 2) and BMI via the respective sol–gel process and addition reaction. Thermal behaviors of these highly crosslinked NLO materials were studied with differential scanning calorimetry (DSC) and thermogravimetric analysis (TGA), respectively. Phase homogeneity and morphology were

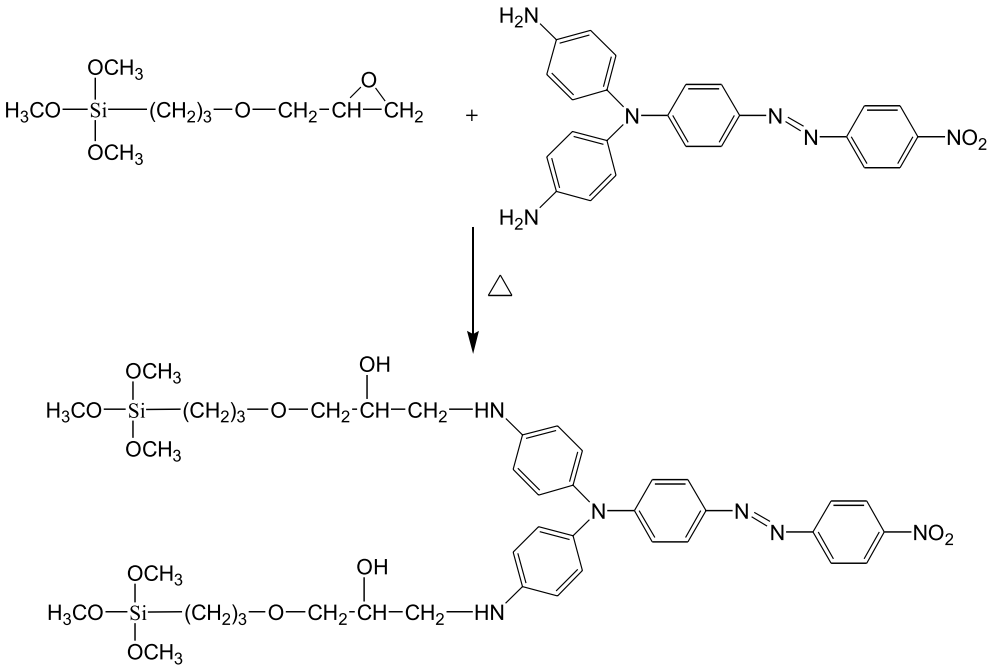

Scheme 2. Synthesis of the alkoxysilane dye (ASD).

analyzed using atomic force microscopy (AFM). Furthermore, the composition effect on the dynamic thermal and temporal stabilities of the NLO properties was also studied.

## 2. Experimental

All of the chemicals were purchased and used as received unless otherwise stated. The solvents were purified by distillation under reduced pressure over calcium hydride. Infrared spectra were recorded by using a Perkin Elmer Paragon 500 FT-IR Spectrophotometer. $^1$H-NMR spectra were obtained with a Brüker AMX400 NMR Spectrometer. Elemental analysis (EA) was performed on an F002 Heraeus CHN–O Rapid elemental analyzer employing acetanilide as a standard. DSC and TGA were performed on a Seiko SII model SSC/5200. A heating rate of 10 °C/min under nitrogen atmosphere was used for DSC. TGA was measured by heating the samples at a heating rate of 10 °C/min under air. Thermal degradation temperature ($T_d$) is taken at 5% weight loss. UV–Vis spectra were recorded on a Perkin Elmer Lambda 2S spectrophotometer. The morphology of the polymer films was also analyzed by AFM (Seiko SPI3800N, Series SPA-400).

### *2.1. Synthesis of maleimide-containing and alkoxysilane-attaching chromophores*

#### *2.1.1. Synthesis of MIDO3*

Disperse Orange 3 (DO3) was purchased from Aldrich Chemical Co. and recrystallized from a mixture of methanol and $H_2O$ prior to the synthesis of MIDO3. Under nitrogen atmosphere, the DO3 (10 g, 0.04 mol) and maleic anhydride (4.45 g, 0.045 mol) were dissolved in ice-bathed 100 ml chloroform, and stirred for 24 h. Then the reaction temperature was raised to 80 °C. Subsequently, sodium acetate (3.28 g, 0.04 mol) and acetic anhydride (8.16 g, 0.08 mol) were added into the reaction solution. The solution was stirred at this temperature for 6 h. The MIDO3 was separated and purified by several re-precipitations from chloroform solution into the mixture of methanol and $H_2O$, and then dried under vacuum. Yield: 70.8%; $^1$H-NMR (DMSO-d6, $\delta$ = ppm): 7.25 (s, 2H, maleimide group), 7.63 ~ 8.50 (m, 8H, aromatic proton); Anal. Calcd. For $C_{16}H_{10}N_4O_4$: C, 59.63%; H, 3.13%; N, 17.38%; O, 19.86%. Found: C, 59.41%; H, 2.99; N, 17.82%; O, 19.78%. FT-IR (KBr): 3100 cm$^{-1}$ [$\nu$ = C–H]; 1722 cm$^{-1}$ [imide C=O]; 1146 cm$^{-1}$ [$\nu$C–N–C]; 842, 692 cm$^{-1}$ [$\delta$C=C, $\delta$C=C–H(*cis*)].

#### *2.1.2. Synthesis of MIANB*

A bulky NLO chromophore, 4-(*N*,*N*-bis(*p*-aminophenyl) amino)-4′-nitroazobenzene (ANB) was synthesized according to literature [23]. This chromophore possesses a $T_d$ higher than 300 °C. Under nitrogen atmosphere, the NLO chromophore (ANB) (0.848 g, 2 mmol) and maleic anhydride (0.4 g, 4.9 mmol) were dissolved in ice-bathed 100 ml DMF, and stirred for 24 h. Then the reaction temperature was raised to 80 °C. Subsequently, sodium acetate (0.164 g, 2 mmol) and acetic anhydride (0.408 g, 4 mmol) were added into the reaction solution. The solution was stirred at this temperature for 6 h. The MIANB was separated and purified by recrystallization from methanol, and then dried under vacuum. Yield: 80.6%; $^1$H-NMR (DMSO-d6, $\delta$ = ppm): 7.18(4H, maleimide group), 6.20 ~ 8.40 (m, 16H, aromatic proton); Anal. Calcd. For $C_{32}H_{20}N_6O_6$: C,

65.75%; H, 3.45%; N, 14.38%; O, 16.42%. Found: C, 65.07%; H, 4.18%; N, 13.77%; O, 16.98%. FT-IR (KBr): 3102 $cm^{-1}$ [$\nu$ = C–H]; 1718 $cm^{-1}$ [imide C=O]; 1136 $cm^{-1}$ [$\nu$C–N–C]; 834, 690 $cm^{-1}$ [$\delta$C=C, $\delta$C=C–H(*cis*)].

### 2.1.3. Synthesis of ASD

The ASD (Scheme 2) was synthesized by the coupling of a monoepoxy of (3-glycidoxypropyl) trimethoxysilane and the above-mentioned chromophore [24]. A bulky NLO chromophore (ANB) (0.445 g, 1.05 mmol) and (3-glycidoxypropl) trimethoxysilane (0.472 g, 2 mmol) were placed in a round bottom flask which was immersed in an oil bath. Then the reaction temperature was raised to 160 °C and stirred at this temperature for 4 h. The ASD was purified by vacuum sublimation. Anal. Calcd. For $C_{42}H_{60}N_6O_{12}Si_2$: C, 56.23%; H, 6.74%; N, 9.37%; O, 21.40%. Found: C, 55.54%; H, 7.05%; N, 9.36%; O, 20.94%.

## 2.2. Syntheses of prepolymers

### 2.2.1. BMI prepolymer

The solution of BMI (3.58 g, 10 mmol) in freshly distilled dimethylacetamide (DMAc) was heated at about 100 °C under nitrogen. Then 2-ethyl-4-methyl-imidazole (EMI, 0.0358 g, 0.3 mmol) was added into the solution. And the solution was kept for another 3 h. The BMI prepolymer was separated and purified by several re-precipitations from DMAc solution into the mixture of methanol and $H_2O$, and then dried under vacuum.

### 2.2.2. MIDO3 containing BMI prepolymer

The MIDO3 containing BMI prepolymer was prepared in the same manners as Section 2.2.1 with a composition of MIDO3 (1.0 g, 3 mmol) and BMI (1.0 g, 0.0028 mol).

### 2.2.3. MIANB containing prepolymers

The MIANB containing BMI prepolymers were prepared in the same manners as Section 2.2.1 with various compositions.

## 2.3. Thin film preparation

The MIANB containing prepolymers and BMI prepolymers with ASD were, respectively, dissolved in the THF. The compositions for these samples based on maleimides are shown in Table 1. The polymer solution was stirred at room temperature for 3 h, and filtered through a 0.45 μm syringe filter. Thin films were prepared by spin-coating the filtered polymer solution onto indium tin oxide (ITO) glass substrates. Prior to poling process, these thin films were dried in a vacuum at room temperature for 24 h.

Table 1
Compositions of the NLO materials based on maleimides

| Sample | Composition (weight ratio) |
|---|---|
| BMI | BMI/MIDO3 (100/0) |
| BMIDO350 | BMI/MIDO3 (50/50) |
| BMIANB10 | BMI/MIANB (90/10) |
| BMIANB30 | BMI/MIANB (70/30) |
| BMIANB50 | BMI/MIANB (50/50) |
| BMIANB70 | BMI/MIANB (30/70) |
| BMIANB90 | BMI/MIANB (10/90) |
| MIANB | BMI/MIANB (0/100) |
| BMIASD10 | BMI/ASD (90/10) |
| BMIASD30 | BMI/ASD (70/30) |
| BMIASD50 | BMI/ASD (50/50) |
| BMIASD70 | BMI/ASD (30/70) |
| BMIASD90 | BMI/ASD (10/90) |
| ASD | BMI/ASD (0/100) |

## 2.4. Poling process and second harmonic generation measurement

The poling process for the second-order NLO polymer films was carried out using an in situ poling technique. The details of the corona poling set-up were the same as was reported earlier [25]. The corona current was maintained at

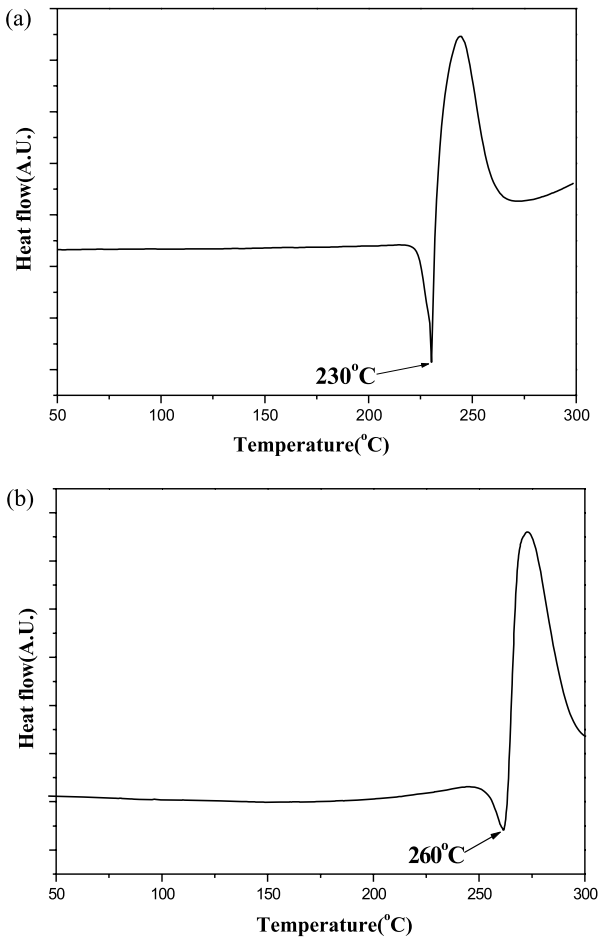


Fig. 2. DSC thermograms of (a) MIDO3 and (b) MIANB.

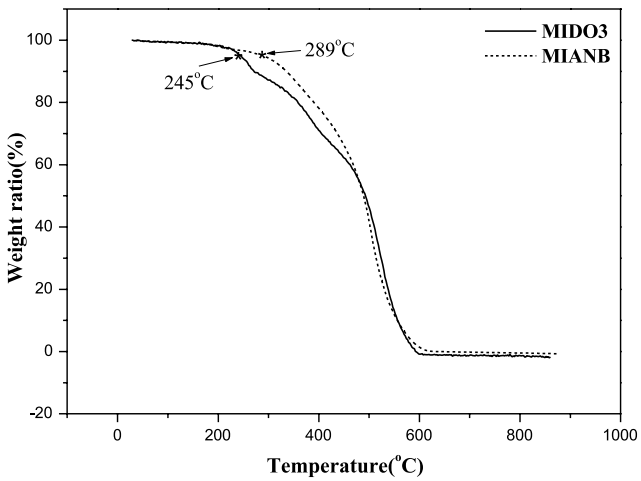


Fig. 3. TGA thermograms of MIDO3 and MIANB.

4 μA with a potential of approximately 5.5 kV while the optimized poling temperature was kept for a certain period of time. The formation of the network and the molecular alignment of the poled order proceeded simultaneously during this period. Upon saturation of the SHG signal intensity, the sample was then cooled down to room temperature in the presence of the poling field at which point the poling field was terminated. The thickness and indices of refraction were measured by a prism coupler (Metricon-2010) for the NLO polymer films. Second harmonic generation measurements were carried out with a Q-switched Nd/YAG laser operating at 1064 nm. Measurement of the second harmonic coefficient, $d_{33}$, has been previously discussed [26], and the $d_{33}$ values were corrected for absorption [27].

## 3. Results and discussion

### 3.1. Thermal properties of the NLO chromophores

DSC was utilized to investigate the melting points and thermal stability of the maleimide-based NLO chromophores. The MIDO3 and MIANB exhibited melting points of 230 and 260 °C, respectively (Fig. 2). Right after melting, the maleimide functionality proceeds to the addition reaction [28]. It is critical that the $T_d$'s of the maleimide-based NLO chromophores should be high enough to undergo high poling temperatures for an extended period of time. The $T_d$'s of the MIDO3 and MIANB samples are 245 and 289 °C, respectively (Fig. 3). These $T_d$'s are higher than those of commercially available NLO chromophores such as Disperse Orange 3 ($T_d$ = 235 °C), and Disperse Red 1 ($T_d$ = 241 °C) [29].[1] It is important to note that no reaction peak (i.e. exothermic peak) was observed for the cured

[1] The $T_d$ values of the commercial azo chromophores Disperse Orange 3 and Disperse Red 1 were observed by detecting 5% weight loss using a Seiko SSC5200 thermogravimetric analyzer under air.

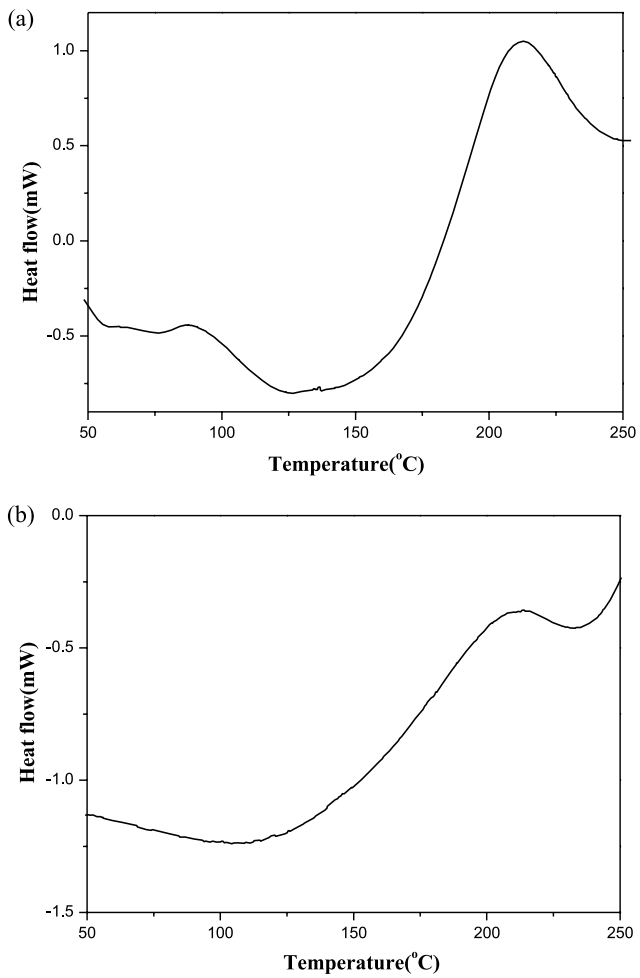


Fig. 4. DSC thermograms of BMIANB50 and BMIASD50 prepolymers.

MIDO3 and MIANB samples as the temperature proceeded up to 300 °C. This indicates that the cured MIDO3 and MIANB samples are thermally stable up to 300 °C.

### 3.2. Optimization of poling and curing conditions

The curing conditions were determined using DSC reaction scans (Fig. 4). For the BMIANB prepolymer, a $T_g$ of about 100 °C was observed. Furthermore, the reaction started at 150 °C, and peaked at 210 °C. On the other hand, the reaction started at 120 °C, and peaked at 205 °C for the BMIASD prepolymer. Moreover, to optimize the poling temperature and investigate the chromophore stability in the polyimide, an UV–Vis spectrophotometer was employed to trace the absorption maximum ($\lambda_{max}$) of the chromophore. Fig. 5 shows absorbance changes of $\lambda_{max}$ (550 nm) for the BMIANB50 and BMIASD50 samples thermal-treated at various temperatures for 30 min, respectively. A sharp decrease of the absorbance was observed when temperatures were higher than 220 °C for these two samples. On the basis of the consideration of the thermal stability of MIANB and ASD, extent of curing, and effective alignment of the NLO chromophores, an optimized poling/curing condition was

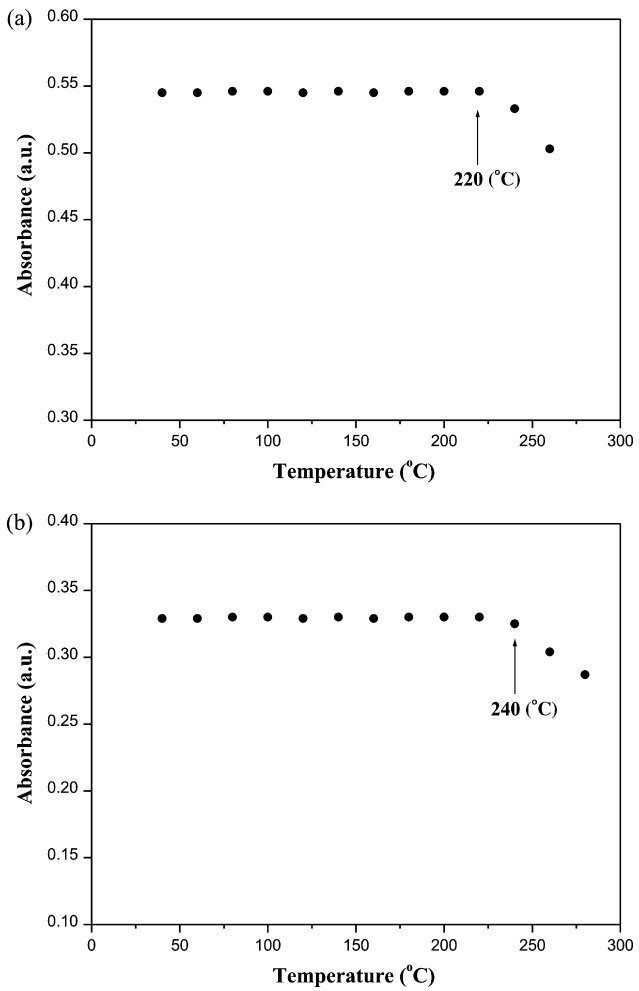


Fig. 5. Thermal stability of the cured (a) BMIANB50 and (b) BMIASD50 samples measured by an UV–Vis spectrophotometer.

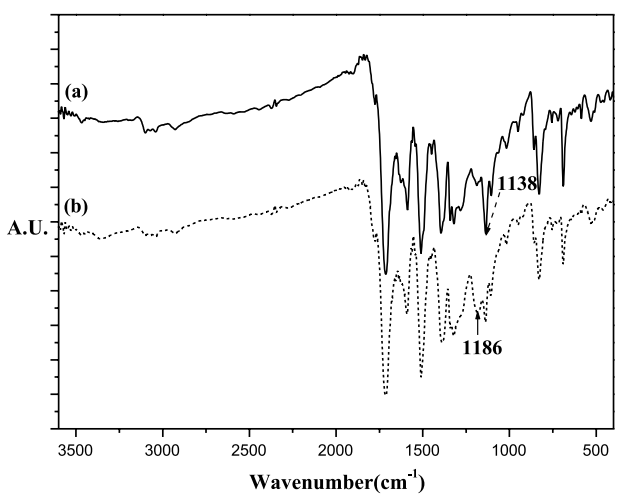


Fig. 6. Infrared spectra of the (a) BMIANB50 prepolymer and (b) cured BMIANB50 sample.

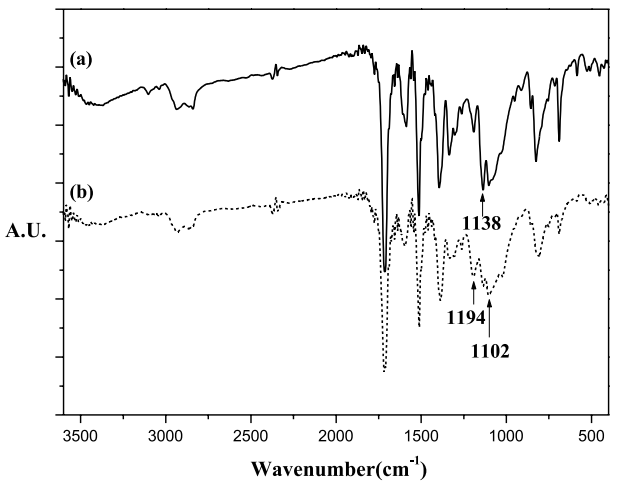


Fig. 7. Infrared spectra of the (a) BMIASD50 prepolymer and (b) cured BMIASD50 sample.

chosen as follows: the polymer films were precured at 140 °C for 1 h, respectively. The samples were then poled in three continuous steps such as poling at 160 °C for 30 min, 180 °C for 30 min, and 200 °C for 2 h. Subsequently, the poled polymer films were cooled to room temperature in the presence of the electric field.

### 3.3. Polymer characterization

FTIR spectra of the BMIANB50 prepolymer and its cured sample are shown in Fig. 6. A very strong peak at 1138 $cm^{-1}$ is associated with $\nu_{C-N-C}$ of the maleimide ring (Fig. 6(a)). On the other hand, a newly emerged band at 1186 $cm^{-1}$ in Fig. 6(b). This is due to the formation of the succinimide ring resulting from addition reaction. Fig. 7 shows the FTIR spectra of the BMIASD50 prepolymer and its cured samples. For the cured BMIASD50 sample, the broadening absorption peak at around 1100 $cm^{-1}$ was identified as the formation of Si–O–Si network resulted from sol–gel reaction among ASD molecules [12]. This is also confirmed by the decreased intensity of the absorption

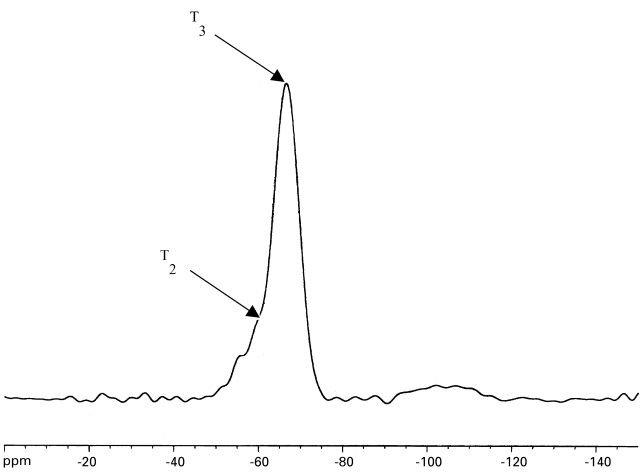


Fig. 8. $^{29}$Si spectrum of the cured BMIASD50 sample.

Table 2
Thermal properties of the maleimide-based NLO materials

| Sample | $T_g$ (°C) | $T_d$ (°C)[a] |
|---|---|---|
| BMI | 250 | 445 |
| BMIDO350 | 193 | 362 |
| BMIANB10 | [b] | 399 |
| BMIANB30 | [b] | 365 |
| BMIANB50 | [b] | 352 |
| BMIANB70 | [b] | 349 |
| BMIANB90 | [b] | 341 |
| MIANB | [b] | 317 |
| BMIASD10 | 275 | 404 |
| BMIASD30 | 270 | 351 |
| BMIASD50 | [b] | 320 |
| BMIASD70 | [b] | 298 |
| BMIASD90 | [b] | 286 |
| ASD | [b] | 285 |

[a] $T_d$ was read at the temperature corresponding to 5% weight loss by TGA.
[b] $T_g$ was not detectable.

peak of hydroxyl stretching around 3400 $cm^{-1}$ after curing. Moreover, formation of covalent bonds among maleimide functional groups is confirmed by the increased intensity of absorption peak at 1194 $cm^{-1}$ (succinimide ring) along with disappearing absorption peak of maleimide ring at 1138 $cm^{-1}$ after curing. The FTIR results demonstrated the respective reactions of the BMI and ASD proceeded simultaneously during the optimized curing process.

To further understand the degree of crosslinking reaction among ASD molecules in polybismaleimide, the silica network of the cured BMIASD50 sample was characterized by $^{29}$Si-NMR (Fig. 8). Two major absorption peaks were observed and assigned to monohydroxy-substituted silica ($T_2$) and nonhydroxy-substituted silica ($T_3$). The stronger absorption intensity of $T_3$ indicates that most of the silicons are bound to two other silicons through the oxygen bridges for the cured BMIASD50 sample [30].

Thermal properties of the maleimide-based materials are shown in Table 2. $T_g$'s of the maleimides-based materials

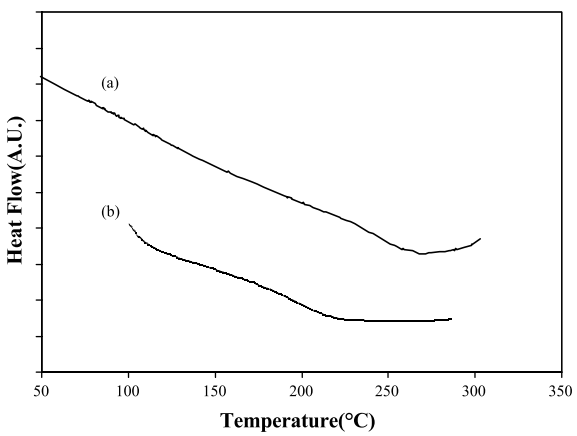


Fig. 9. DSC thermograms of the cured (a) BMI and (b) BMIDO350 samples.

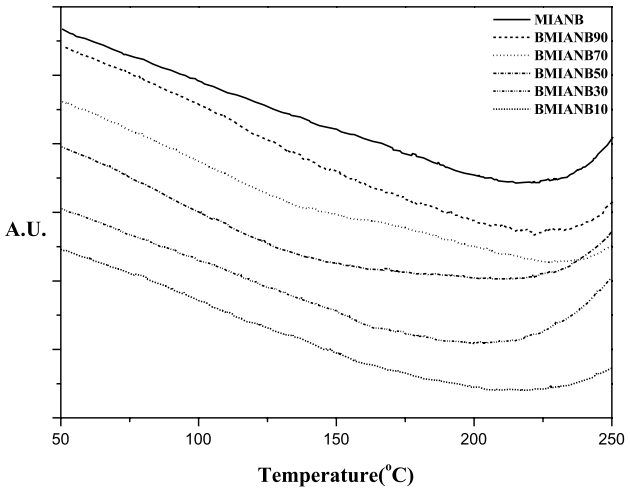


Fig. 10. DSC thermograms of the cured BMIANB samples.

were measured on the DSC after the above-mentioned curing process. $T_g$'s of the cured BMI and BMIDO350 were observed at 250 and 193 °C, respectively (Fig. 9). However, $T_g$'s were not detectable from the DSC study for the cured BMIANB samples possibly due to the formation of high crosslinking density of the organic networks (Fig. 10) [31]. For the cured BMIASD samples, $T_g$'s of 275 and 270 °C were observed for BMIASD10 and BMIASD30 samples, respectively (Table 2 and Fig. 11). As the content of ASD increased, the glass transition became broad and indistinct. This is because of the formation of high crosslinking density of the intertwined organic and inorganic networks [31]. It is important to note that the $T_g$'s of the cured BMIASD10 and BMIASD30 samples are somewhat higher than that (250 °C) of the cured BMI sample Moreover, the glass transition zones of the cured BMIASD10 and BMIASD30 samples are also much broader and indistinct. This further confirms the formation of a high crosslinked density for the organic–inorganic networks, resulting in a net decrease in both the chain mobility and vibrational activity [31–33]. In fact, the cured BMIASD samples are in the form of IPN.

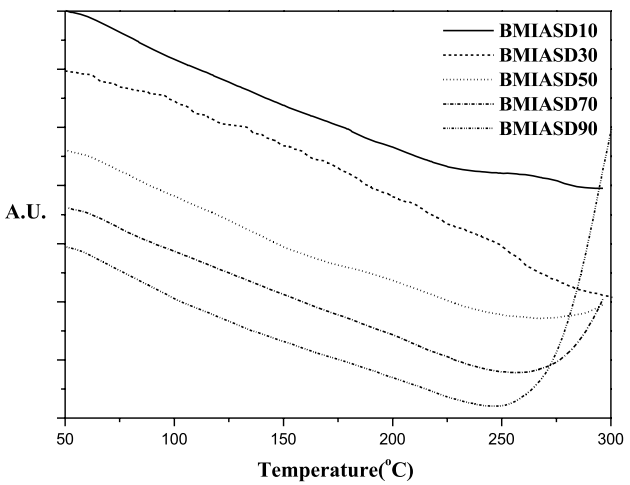


Fig. 11. DSC thermograms of the cured BMIASD samples.

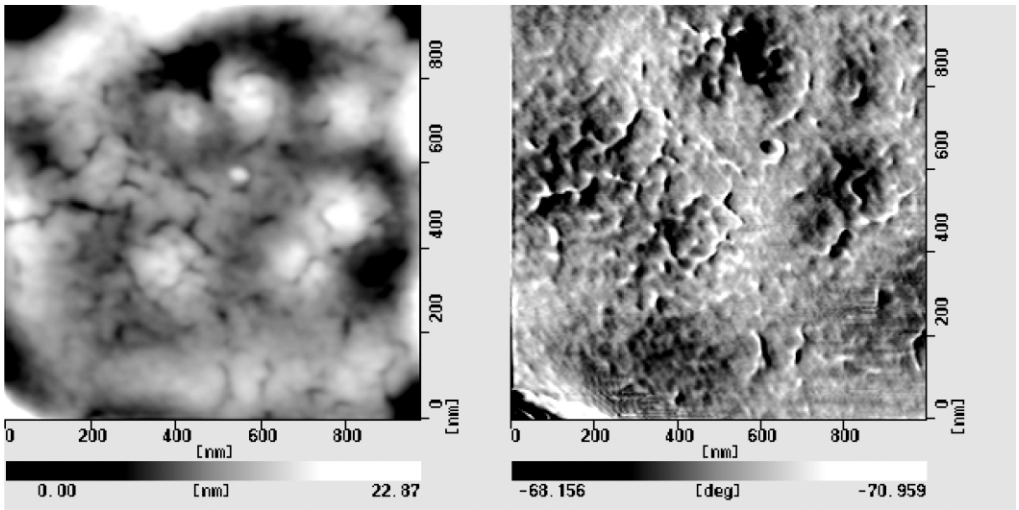


(a)

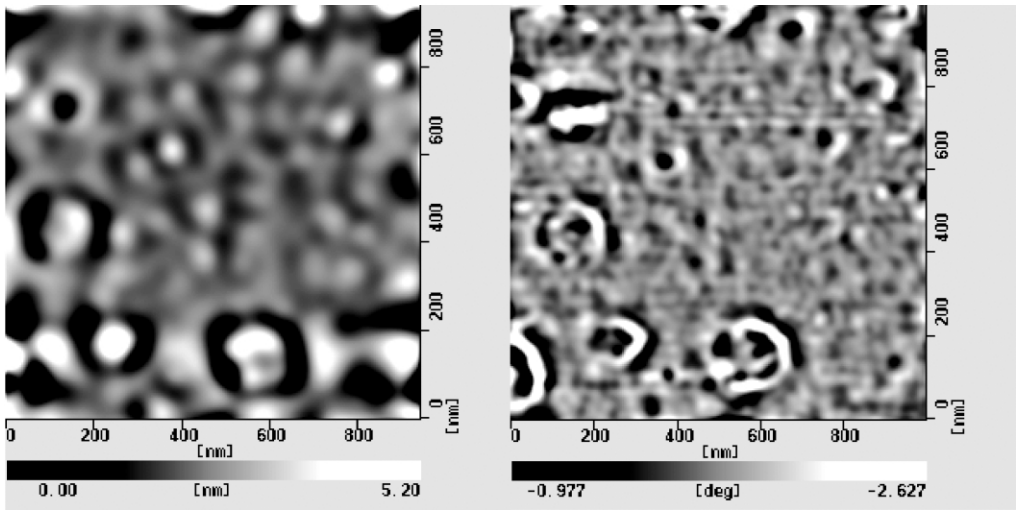


(b)

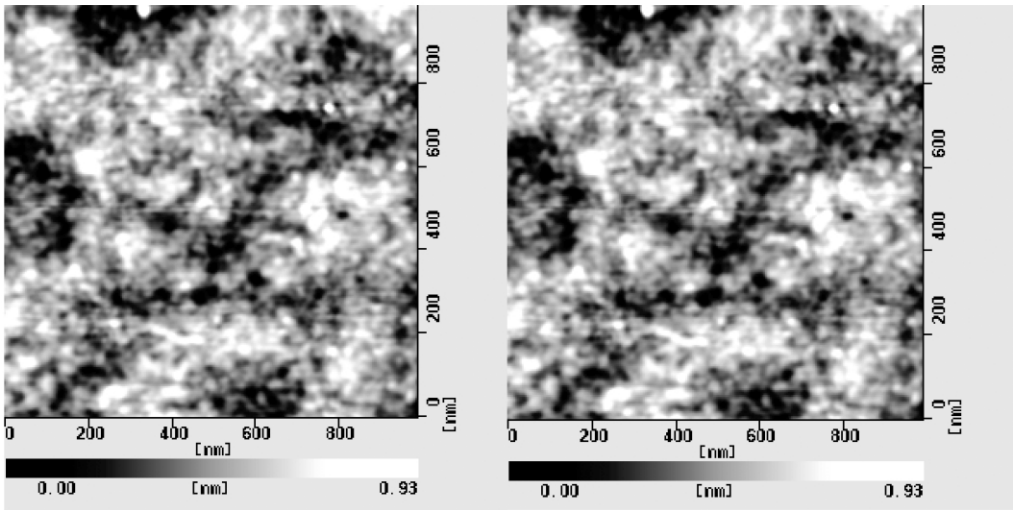


(c)

Fig. 12. AFM topography images (left) and phase images (right) of the cured samples (a) BMIASD10, (b) BMIASD50, and (c) BMIASD90.

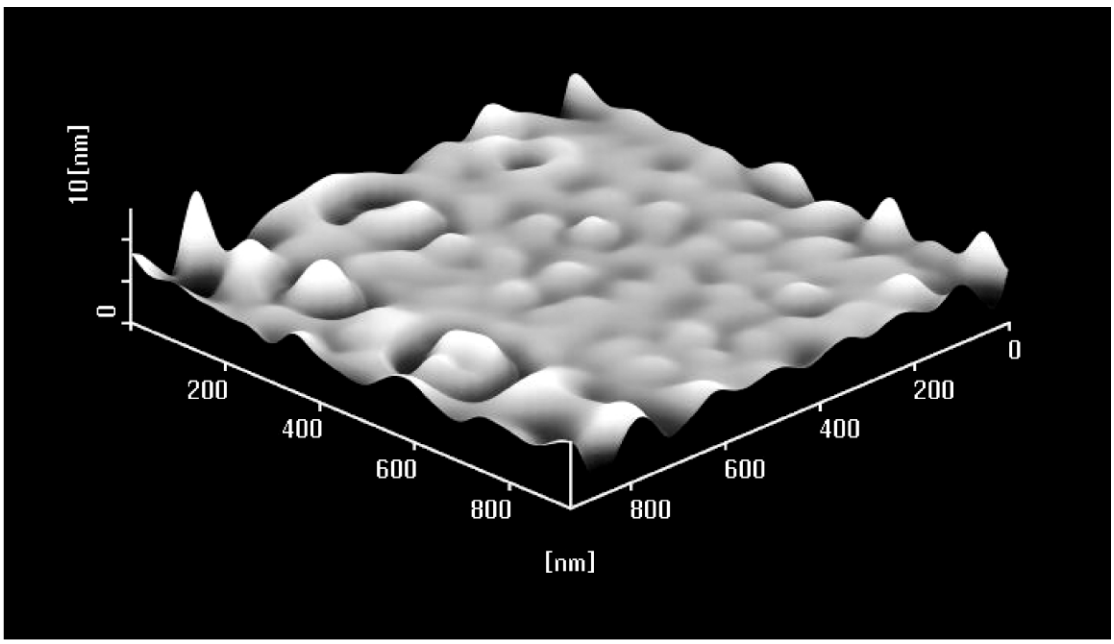


(a)

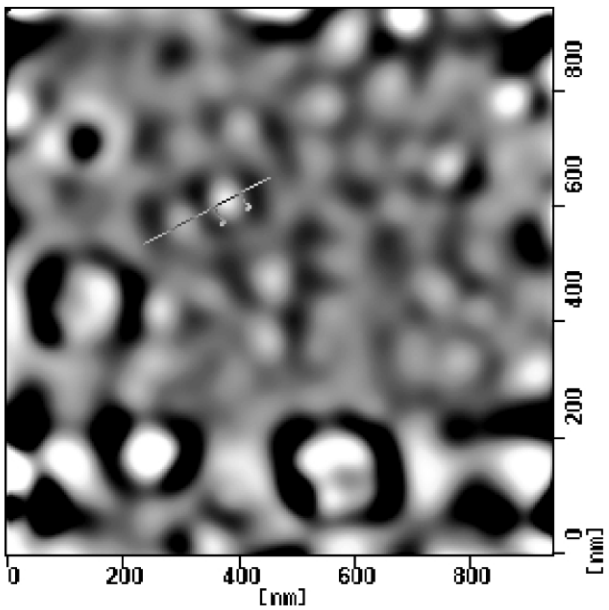


(b)

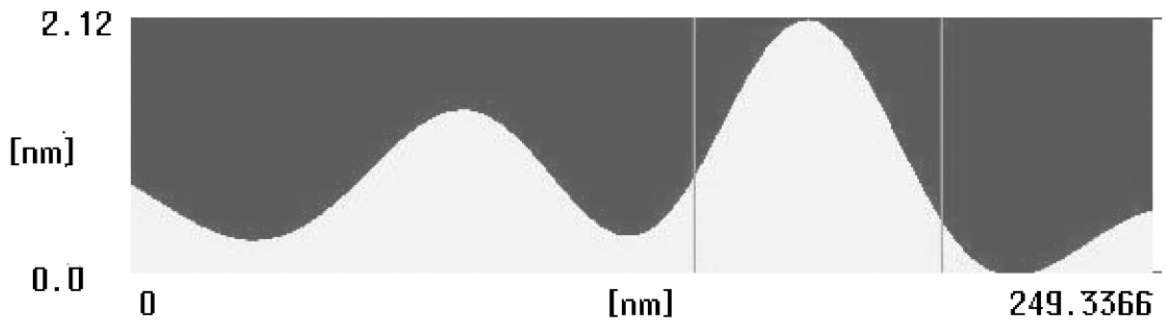


(c)

Fig. 13. (a) AFM topography image (3D-display), (b) AFM topography image, and (c) crosssectional image on the line in (b) for the cured BMIASD50 sample.

In IPN, the molecular motion of each polymer is further restricted due to the entanglements between two different networks [22]. In addition, thermal decomposition behavior was measured on a TGA under air after curing. $T_d$ was read at the temperature corresponding to the weight loss of 5%. The $T_d$'s of the cured BMIANB and BMIASD materials are also summarized in Table 2. $T_d$'s were observed at temperatures above 310 °C for the cured MIANB containing BMI samples. The $T_d$ decreased with increasing MIANB content. Moreover, $T_d$'s of the cured BMIASD samples were observed in the range of 286–404 °C. The $T_d$ decreased with increasing ASD content. Yet, all of the cured BMIASD samples have higher $T_d$'s than that of the cured ASD ($T_d$ = 285 °C). It is important to note that the 5% weight loss of the NLO materials mostly results from either further sol–gel reaction (i.e. condensation) of residual silanol groups [34], or degradation of the NLO moieties (i.e. azobenzene).

The homogeneity of the organic–inorganic IPN materials (i.e. the cured BMIASD samples) was studied using the tapping mode AFM. The tapping mode AFM morphology and phase images were obtained to characterize local properties of the surface. Numerous small grains could be observed spreading on the entire surface area, with a minor surface roughness of 1–23 nm (Fig. 12). To observe these small grains more precisely, crosssectional analysis of the AFM scan was also carried out (Fig. 13). It is found that the domain sizes of these cured BMIASD samples are in the range of 60–150 nm. The observation by AFM supports that the inorganic networks are distributed throughout the polymer matrices on the molecular scale [35].

### 3.4. Optical properties

To investigate the absorption behavior as a function of time, the absorption spectra was taken regularly over 190 h period under thermal treatment at 100 °C for the poled/cured BMIANB50 and BMIASD samples (Fig. 14). The maximum of the absorption was located around 550 nm for the untreated BMIANB50 and BMIASD samples, respectively. Immediately after poling/curing, a decrease in absorption and a blue shift were observed in the spectrum. This was due to dichroism and electrochromism resulting from the induced dipole alignment [36]. During the next 190 h, the absorption spectra remained unchanged for all samples. The linear optical properties of these NLO sol–gel materials are summarized in Table 3. The thickness of the polymer films is ranged from 0.7 to 1.1 μm. The refraction indices are ranged from 1.65 to 1.76. The second-harmonic coefficients $d_{33}$ and $d_{31}$ of poled/cured ASD, BMIANB, and BMIASD samples for incident light of 1064 nm are summarized in Table 4. These maleimide-based materials show large second-order nonlinearity after poling and curing. Moreover, the second-harmonic coefficients increase with increasing content of NLO chromophores linearly (Fig. 15).

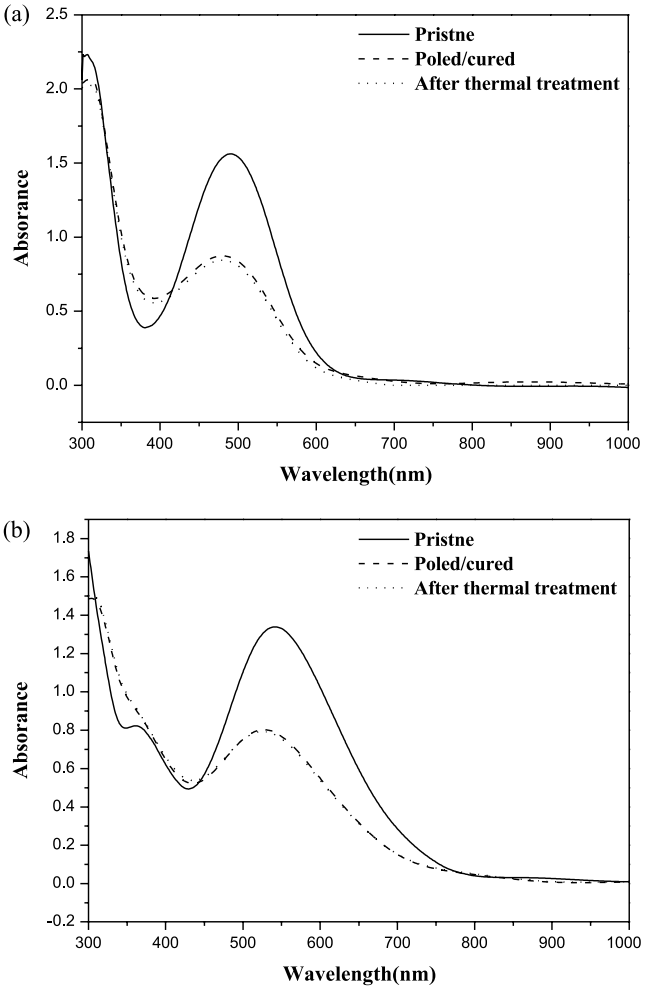


Fig. 14. UV/Vis absorption spectra of the cured (a) BMIANB50 and (b) BMIASD50 samples.

This means aggregation of NLO chromophores does not occur in the above measured systems.

In general, the effective second harmonic coefficient ($d_{eff}$) of NLO polymers remained stable at low temperatures,

Table 3
Thickness and refraction indices of the maleimide-based NLO materials

| Sample | $d$ (μm)[a] | $n_{543}$[b] | $n_{633}$ | $n_{830}$ |
|---|---|---|---|---|
| BMIDO350 | 1.1 | 1.70 | 1.68 | 1.65 |
| BMIANB10 | 0.9 | 1.76 | 1.75 | 1.73 |
| BMIANB30 | 0.7 | 1.73 | 1.72 | 1.70 |
| BMIANB50 | 0.9 | 1.73 | 1.70 | 1.68 |
| BMIANB70 | #[c] | # | # | # |
| BMIANB90 | # | # | # | # |
| BMIASD10 | 0.9 | 1.70 | 1.67 | 1.65 |
| BMIASD30 | 0.8 | 1.72 | 1.70 | 1.67 |
| BMIASD50 | 0.8 | 1.73 | 1.72 | 1.71 |
| BMIASD70 | 0.9 | 1.74 | 1.72 | 1.71 |
| BMIASD90 | 1.1 | 1.75 | 1.73 | 1.71 |
| ASD | 0.7 | 1.76 | 1.74 | 1.72 |

[a] The thickness of polymer film.
[b] $n_{543}$, $n_{633}$, $n_{830}$: refraction indices at 543, 633, and 830 nm, respectively.
[c] Not available due to opaqueness of polymer films.

Table 4
Second harmonic coefficients $d_{33}$ and $d_{31}$ (pm/V) of the poled/cured maleimide-based NLO materials at 1064 nm

| Sample | $d_{33}$ | $d_{31}$ |
|---|---|---|
| BMIDO350 | 8.3 | 3.3 |
| BMIANB10 | 6.9 | 3.8 |
| BMIANB30 | 18.3 | 8.3 |
| BMIANB50 | 30.0 | 7.7 |
| BMIANB70 | #[a] | # |
| BMIANB90 | # | # |
| BMIASD10 | 5.9 | 2.5 |
| BMIASD30 | 14.7 | 5.9 |
| BMIASD50 | 23.1 | 8.3 |
| BMIASD70 | 36.5 | 10.4 |
| BMIASD90 | 44.7 | 18.1 |
| ASD | 57.0 | 21.7 |

[a] Not available due to opaqueness of polymer films.

but decayed significantly at a specific temperature. This specific temperature is defined as the effective relaxation temperature, $T_0$ [37,38]. The $T_0$ value provides information on maximum device operating temperatures that the film can endure, and allows quick evaluation of the temporal and thermal stability of the materials. Fig. 16 shows the dynamic NLO thermal stability of the poled/cured BMIDO350, BMIANB50 and BMIASD50 samples. The $T_0$ (148 °C) of

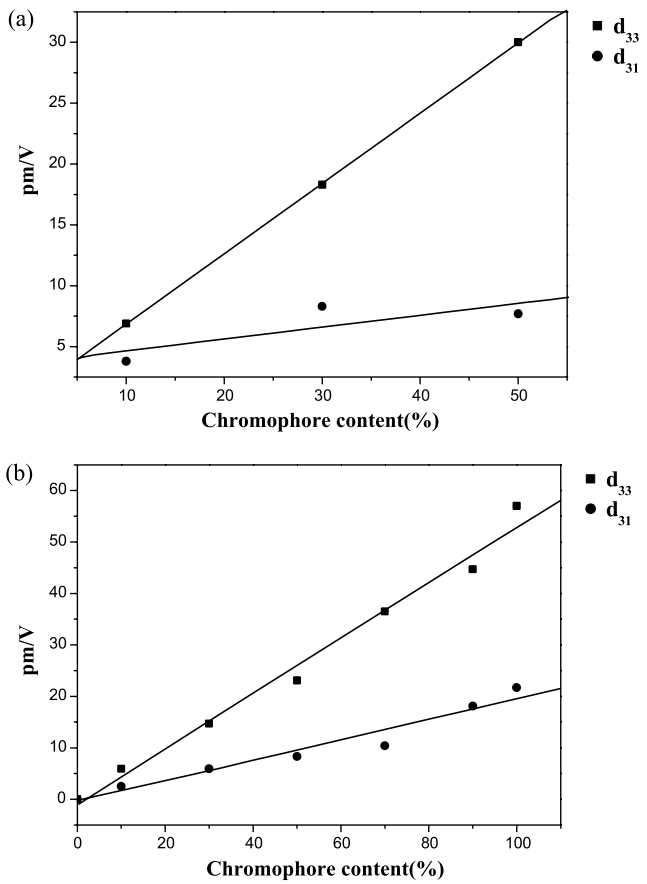


Fig. 15. Second harmonic coefficient plotted as a function of chromophore content for the poled/cured (a) BMIANB50 and (b) BMIASD50 samples.

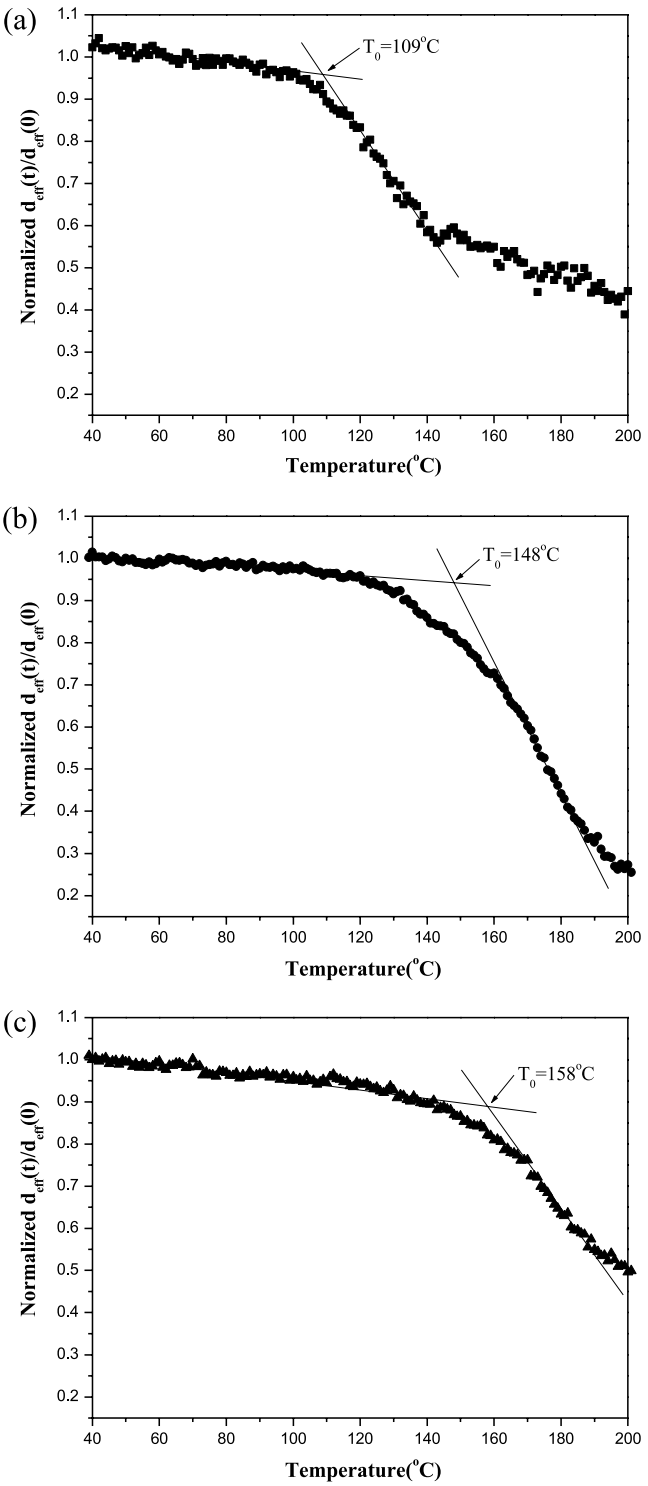


Fig. 16. Temperature dependence of the dipole re-orientational dynamics of the poled/cured (a) BMIDO350, (b) BMIANB50, and (c) BMIASD50 samples.

the poled/cured BMIANB50 sample is much higher than that (109 °C) of the poled/cured BMIDO350 sample. This is possibly because the chromophore size of ANB is much larger than that of DO3. This is further confirmed by a much higher $T_0$ (158 °C) for the poled/cured BMIASD50 sample.

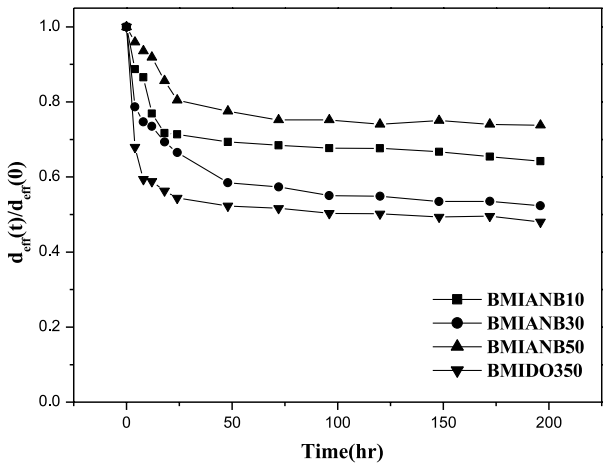


Fig. 17. Temporal behavior of the effective second harmonic coefficient for the poled/cured BMIDO350, BMIANB10, BMIANB30, and BMIANB50 samples at 100 °C.

The $T_0$ is about 10 °C higher than that of the poled/cured BMIANB50 sample with similar NLO density. This indicates that the entanglements between different networks of IPN system are somewhat more effective to restrict the mobility of the aligned NLO chromophores as compared to the interchain crosslinking system (i.e. the poled/cured BMIANB system), despite that the NLO chromophores in this interchain crosslinking system are rigidly tethered in the polymer chains. On the other hand, the NLO chromophores are separated from inorganic networks by a soft linkage in the IPN system.

The $d_{eff}$ temporal characteristics for the poled/cured BMIANB samples at 100 °C are shown in Fig. 17. The initial decay of a few percent in the $d_{eff}$ value at 100 °C is a result of the initial loss of orientation, perhaps of the uncrosslinked components [9]. A much better temporal stability was obtained for the poled/cured BMIANB samples as compared to the poled/cured BMIDO350 sample. After being subjected to thermal treatment at 100 °C for 190 h, a reduction of less than 50% in $d_{eff}$ was observed for all of the poled/cured BMIANB samples. For the poled/cured BMIASD IPN samples, the BMIASD10 and BMIASD30 samples exhibited better temporal stability (Fig. 18). The temporal stability was decreased with increasing content of ASD. Nevertheless, a reduction of less than 30% in $d_{eff}$ was observed for all of the poled/cured BMIASD samples after being subjected to thermal treatment at 100 °C for 190 h. It is important to note that a reduction of 70% in $d_{eff}$ was observed for the poled/cured ASD sample (Fig. 18). In comparison with the poled/cured BMIANB samples, the poled/cured BMIASD samples exhibited better temporal stability. This is direct consequence of the permanent entanglements between two different networks of the IPN system capable of suppressing the mobility of the aligned NLO chromophores [39–41].

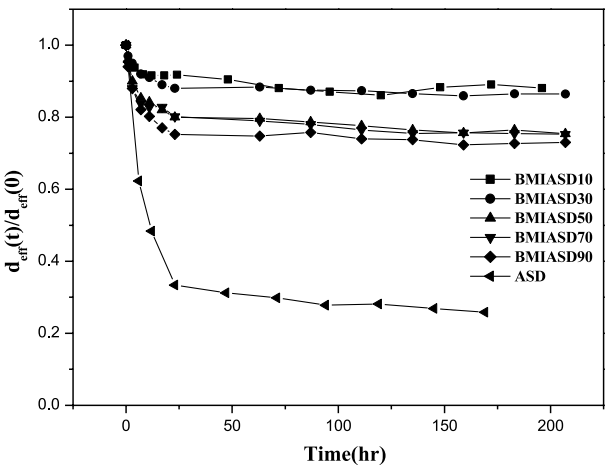


Fig. 18. Temporal behavior of the effective second harmonic coefficient for the poled/cured BMIASD samples at 100 °C.

## 4. Conclusion

A series of the maleimide-based crosslinked organic and organic–inorganic NLO materials have been developed. Large second-order optical nonlinearity (6.9–57.0 pm/V) was obtained after poling and curing. The maleimide containing MIANB was reacted with BMI to form an NLO-active crosslinked polybismaleimide with NLO chromophores tethered onto the polymer main chains, whereas the simultaneous sol–gel reaction of ASD, and addition reaction of BMI prepolymer lead to an NLO-active IPN system. The entanglements between two different networks of IPN system were more efficient to suppress the mobility of the aligned NLO chromophores than the interchain crosslinking BMIANB system. Consequently, the IPN system exhibited much better dynamic thermal and temporal stabilities than the organic crosslinked system. Future work involves the synthesis of double-end crosslinkable ASD or chromophore to further enhance the nonlinearity as well as temporal stability [42–44].

## Acknowledgements

The authors thank the National Science Council of Taiwan, ROC (Grant NSC89-2216-E-005-022) and Chung-Shan Institute of Science and Technology for financial support.

## References

[1] Prasad PN, Williams DJ. Introduction to nonlinear optical effects in molecules and polymers. New York: Wiley; 1991.
[2] Singer KD, Sohn JE, Lalama SJ. Appl Phys Lett 1986;49:248.
[3] Meredith GR, Dusen JG, Williams DJ. Macromolecules 1982;15:1385.
[4] Wang NP, Leslie TM, Wang S, Kowel ST. Chem Mater 1995;7:185.
[5] Stenger-Smith JD, Henry RA, Hoover JM, Lindsay GA, Nadler MP, Nissan RA. J Polym Sci Polym Chem 1993;31:2899.

[6] Xu C, Wu B, Todorova O, Dalton LR, Shi Y, Ranon PM, Steier WH. Macromolecules 1993;26:5303.
[7] Jeng RJ, Chen YM, Jain A, Tripathy SK, Kuman J. Opt Commun 1992;89:212.
[8] Kim J, Plawsky JL, LaPeruta R, Korenowski GM. Chem Mater 1992; 4:249.
[9] Jeng RJ, Chen YM, Chen JI, Kumar J, Tripathy SK. Macromolecules 1993;26:2530.
[10] Marturunkakul S, Chen JI, Jeng RJ, Sengupta S, Kumar J, Tripathy SK. Chem Mater 1993;5:743.
[11] Wu JW, Valley JF, Ermer S, Binkley ES, Kenney JT, Lipscomb GF, Lytel R. Appl Phys Lett 1991;58:225.
[12] Jeng RJ, Chen YM, Jain AK, Kumar J, Tripathy SK. Chem Mater 1992;4:1141.
[13] Lin JT, Hubbard MA, Marks TJ, Lin W, Wong GK. Chem Mater 1992;4:1148.
[14] Hsiue GH, Kuo JK, Jeng RJ, Chen JI, Jiang XL, Marturunkakul S, Kumar J, Tripathy SK. Chem Mater 1994;6:884.
[15] Updegraff IH. Encyclopedia of polymer science and engineering. New York: Wiley; 1986.
[16] Jeng RJ, Hsiue GH, Chen JI, Marturunkakul S, Li L, Jiang XL, Moody R, Masse C, Kumar J, Tripathy SK. J Appl Polym Sci 1995;55:209.
[17] Landry CJT, Coltrain BK, Wesson JA, Zumbulyadis N, Lippert JL. Polymer 1992;33:1496.
[18] Wu W, Wang D, Zhu P, Wang P, Ye C. J Polym Sci Polym Chem 1999;37:3598.
[19] Lue J, Zhan C, Qin J. React Funct Polym 2000;44:219.
[20] Wang C, Zhang C, Wang P, Zhu P, Wu W, Ye C, Dalton LR. Polymer 2000;41:2583.
[21] Samyu C, Ballet W, Verbiest T, Van Beylen M, Persoons A. Polymer 2001;42:8511.
[22] Marturunkakul S, Chen JI, Li L, Jeng RJ, Kumar J, Tripathy SK. Chem Mater 1993;5:592.
[23] Miller RD, Burland DM, Jurich M, Lee VY, Moylan CR, Thackara JI, Twieg RJ, Verbiest T, Volksen W. Macromolecules 1995;28:4970.
[24] Mandal B, Jeng RJ, Kumar J, Tripathy SK. Macromol Chem Rapid Commun 1991;12:607.
[25] Mortazavi MA, Knoesen A, Kowel ST, Higgins BG, Dienes A. J Opt Soc Am 1989;B6:773.
[26] Jeng RJ, Chen YM, Kumar J, Tripathy SK. J Macromol Sci Pure Appl Chem 1992;A29:1115.
[27] Mandal BK, Chen YM, Lee JY, Kumar J, Tripathy SK. Appl Phys Lett 1991;58:2459.
[28] Liu YL, Liu YL, Jeng RJ, Chiu YS. J Polym Sci, Polym Chem 2001; 39:1716.
[29] Kuo WJ, Hsiue GH, Jeng RJ. Macromolecules 2001;34:2373.
[30] Lee RH, Hsiue GH, Jeng RJ. J Appl Polym Sci 2001;79:1852.
[31] Stevens G, Richardson M. Polymer 1983;24:851.
[32] Plazek D, Frund Z. J Polym Sci Polym Phys 1990;28:431.
[33] Augell AC. J Non-Cryst Solids 1991;131:13.
[34] Wung CJ, Lee KS, Prasad PN, Kim JC, Jin JI, Shim HK. Polymer 1992;33:4145.
[35] Wen J, Dhandapani B, Oyama ST, Wilkes GL. Chem Mater 1997;9: 1968.
[36] Yang Z, Xu C, Wu B, Dalton LR, Kalluri S, Steier WH, Shi Y, Bechtel JH. Chem Mater 1994;6:1899.
[37] Tsutsumi N, Moridhima M, Sakai W. Macromolecules 1998;31:7764.
[38] Hsiue GH, Kuo WJ, Lin CH, Jeng RJ. Macromol Chem Phys 2000; 201:2336.
[39] Hsieh KH, Liao DC, Chen CY, Chiu WY. Polym Adv Technol 1996; 7:265.
[40] Han X, Chen B, Guo F. IPNs around the world, science and engineering. New York: Wiley; 1997.
[41] Xie HQ, Hung XD, Guo JS. Polymer 1996;37:771.
[42] Kim HK, Kang SJ, Choi SK, Min YH, Yoon CS. Chem Mater 1999; 11:779.
[43] Kim EH, Moon IK, Kim HK, Lee MH, Han SG, Yi MH, Choi KY. Polymer 1999;40:6157.
[44] Kuo WJ, Hsiue GH, Jeng RJ. Macromol Rapid Commun 2001;22(8): 601.